Hindawi Publishing Corporation
Journal of Nanotechnology
Volume 2013, Article ID 939531, 6 pages
http://dx.doi.org/10.1155/2013/939531

Research Article

Photocatalytic $BiFeO_3$ Nanofibrous Mats for Effective Water Treatment

Parmiss Mojir Shaibani, K. Prashanthi, Amirreza Sohrabi, and Thomas Thundat

Department of Chemical and Materials Engineering, University of Alberta, Edmonton, AB, Canada T6G 2V4

Correspondence should be addressed to Parmiss Mojir Shaibani; mojirsha@ualberta.ca

Received 31 January 2013; Revised 9 April 2013; Accepted 8 May 2013

Academic Editor: Jorge Seminario

One-dimensional $BiFeO_3$ (BFO) nanofibers fabricated by electrospinning of a solution of Nylon6/BFO followed by calcination were used for photocatalytic degradation of contaminants in water. The BFO fibers were characterized using scanning electron microscopy (SEM), X-ray diffraction (XRD), and UV-Vis spectroscopy. The SEM images of the as-spun samples demonstrated the successful production of nanofibers and the SEM images of the samples after calcination confirmed the integrity of the continuous BFO nanofibers. XRD analysis indicated the dominant presence of BFO phase throughout the calcinated nanofibers. Photocatalytic activity of the nanofibers and their application in water purification were investigated against 4-chlorophenol (4CP) as a model water contaminant. The results of the UV-Vis spectroscopy show the degradation of the 4CP by means of the photocatalytic activity of the BFO nanofibers. The kinetics of the photodegradation of 4CP is believed to be governed by a pseudo-first-order kinetics model.

1. Introduction

The presence of hazardous nondegradable contaminants in water such as pharmaceuticals [1] and organic and inorganic solutes [2] poses dangers of human and environmental exposure that result in health effects and environmental damage [3, 4]. A widespread need, therefore, exists for developing cost effective and scalable methods to reduce harmful compounds to a permitted amount or eliminate them entirely. Many methods such as the application of polymeric adsorbents, membrane separation, and oxidation treatments have been proposed [5]. Photocatalysis, a well-known oxidation treatment method, has the advantage of direct absorption of light at room temperature where there is no need for thermal activation to fully mineralize pollutants [6, 7]. Photocatalysis involves photolysis, the breaking down of a chemical compound by the assistance of light, which is accelerated by means of a catalyst. This process can occur in the form of homogeneous as well as heterogeneous photocatalysis. In the former, photocatalysts such as ozone are used and the reactants exist at the same phase as the catalyst. In the latter, however, the reactants are in a different phase from the reactive entity that triggers various oxidation and reduction reactions through which the contaminating agent is degraded [7]. Semiconductors are often applied in this type of photocatalysis. In this case, photocatalysis is activated when photons with sufficient energy excite the electrons of the valence band in the photocatalyst creating electron-hole pairs. Due to the presence of contaminants, the recombination of the electrons and holes is delayed, the holes react with the moisture on the surface of the photocatalyst, and a series of oxidative reactions with so-called hole scavengers such as the contaminants are triggered. The electrons in turn participate in a chain of reductive reactions with the oxidants in the environment. In this process the pollutant is degraded into harmless final products such as CO_2 [7].

Several studies have been carried out on the photocatalytic activity of TiO_2 due to its beneficial characteristics such as low cost, water insolubility, and high photocatalytic efficiency due to its high quantum yield. Different structures of TiO_2 have been investigated for photocatalysis that include TiO_2 nanoparticles [8, 9], nanofibers [10], nanotubes [11], thin films [12], and even flower structures [13]. Recently, Choi et al.

demonstrated the superiority of electrospun TiO_2 nanofibers over other structures in terms of hydrogen generation as a result of photocatalytic activity [14]. One apparent advantage of nanofibers over structures such as nanoparticles is that the nanofibers can be used as membranes, and therefore no additional step is needed for the removal of the photocatalysts from the water, especially when treating drinking water. Laera et al. demonstrated that TiO_2 nanofibers were comparable with the commercial TiO_2 Degussa P25 in the degradation of Congo Red (CR) and furthermore concluded that the nanofibers are easily separable from the aqueous medium [15].

The introduction of $BiFeO_3$ (BFO) as one of the few materials exhibiting multiferroic properties at room temperature generated much interest in this semiconductor, and the discovery of the photocatalytic activity of BFO offers new opportunities for the application of BFO in water purification. As band gap values are size dependent, the band gap energy of BFO has been reported to be in the range of 2.5–2.8 eV by Ihlefeld et al. [16] as well as Hauser et al. [17]; however, value of 2.2 eV has also been stated in the literature for nanostructured BFO particles [18]. These reports show that BFO has a smaller band gap compared to the band gap energy of 3.2 eV for TiO_2. Xu et al. reported the degradation of CR by applying BFO thin film under visible light irradiation, which proved to be economic as well as reproducible. Their results indicated an approximate 16% decrease in the contaminant concentration in roughly 240 min [19]. In a similar study, Gao et al. utilized BFO in the forms of bulk and nanoparticles in order to degrade methyl orange under two regimes of irradiation, that is, visible and UV-Vis irradiations. The results presented the decrease in the concentration of the methyl orange under both irradiation regimes and also for both structures; however, the most significant degradation occurred when BFO nanoparticles were utilized under the UV-Vis range exposure. Therefore, decreasing the size of the BFO from bulk to nanoparticles increased the efficiency. Moreover, using a more energetic irradiation with a wavelength in UV-Vis range instead of visible light enhanced the photodegradation of the methyl orange [20]. Notwithstanding the reports, to the best of our knowledge no study has yet been done on the photocatalytic activity of one-dimensional BFO nanostructures in water purification. Given the fact that BFO is a relatively new material and one-dimensional BFO nanostructures have only recently been developed, exploring their benefits in the field of water purification holds great merit.

Here we report on photocatalytic degradation capability of electrospun BFO nanofibers. In this study, 4CP, a harmful organic compound which is found in pesticidal chemical industries, petrochemical industries, and a common chemical intermediate in effluent chlorination, is chosen as a model contaminant [21]. The degradation behavior of 4CP in aqueous solution in the presence of BFO nanofibers under UV irradiation is investigated. The details of electrospinning process and subsequent calcination measures to prepare the nanofibers are presented as well as characterization techniques. The governing kinetics of the photocatalytic process is also explored based on a pseudo-first-order kinetic model.

2. Experimental

2.1. Materials. Pallet-shaped Nylon6 with a 3 mm size, density of 1.084 g/cm^3 at 25°C, and an average molecular weight of 11202 g/mol was purchased (Sigma Aldrich, Canada) along with formic acid with a purity of >98% which acts as the solvent for Nylon6. Bismuth (III) nitrate pentahydrate with a purity of 98% (Acros, USA) and 99.99% pure iron (III) nitrate nonahydrate (Sigma Aldrich, Canada) were obtained in addition to 2-methoxyethanol as a solvent (Acros, NJ, USA), ethanolamine with a purity more than 99.5% purified by redistillation (Sigma Aldrich, Canada), and glacial acetic acid with a purity of 99.7% (Fisher Scientific, Canada). High purity 4-chlorophenol (Sigma Aldrich, Canada) with ≥99% purity was used as a water contaminant.

2.2. Electrospinning Solution. Bismuth (III) nitrate pentahydrate and iron (III) nitrate nonahydrate salts with a 1.05 : 1 w/w ratio were dissolved in 2-methoxyethanol and stirred until a homogeneous solution was obtained. Subsequently, to set the pH of the solution to 4, a sufficient amount of ethanolamine was added. Furthermore, glacial acetic acid was used to control the viscosity of the BFO solution to suit the feasible viscosity range of the sequent electrospinning. The entire BFO sol-gel precursor solution was then magnetically stirred for 2 hrs at room temperature. 15 wt% Nylon6 solution was prepared by dissolving Nylon6 pallets in formic acid and followed by magnetic stirring; the final solution to be electrospun was made by adding the BFO solution drop by drop to the Nylon6 polymer solution with a 1 : 1 v/v ratio while being magnetically stirred to obtain a homogeneous solution.

2.3. Electrospinning Process and Calcination. A homemade electrospinning setup was utilized for the electrospinning of the BFO/Nylon6 solution. A voltage of 20 kV was applied by means of a 25A series Dc-Dc high voltage module (Ultravolt, USA) to the solution through a 21-gauge stainless steel needle. The separation distance between the metallic nozzle and the aluminum collector, which was grounded, was set to be 20 cm. The flow rate of the solution was fixed at 0.3 mL/hr on the syringe pump (Fisher Scientific, Canada), and the electrospinning experiments were conducted at ambient temperature. For the purpose of easily characterizing the electrospun products, $Pt/Ti/SiO_2/Si$ substrates were also attached to the collector. The electrospun material was then dried in a vacuum oven at 125°C for 1 hr and further calcinated at 600°C for a duration of 2 hrs in a furnace in air ambient to eliminate the Nylon6 surrounding the expected BFO nanofibers.

2.4. Characterization. Calcinated samples on $Pt/Ti/SiO_2/Si$ substrates were characterized using X-ray diffraction (XRD) (Rigaku, Japan, Cu K_α radiation $\lambda = 1.5405$ Å) to determine the phase structure; scanning electron microscopy (SEM) (VEGA3, Tescan, USA) with an accelerating voltage of 30 kV was used to examine the morphology of the as-spun samples as well as calcinated samples; the diameter of the fibers prior to and after calcination was also studied. All samples

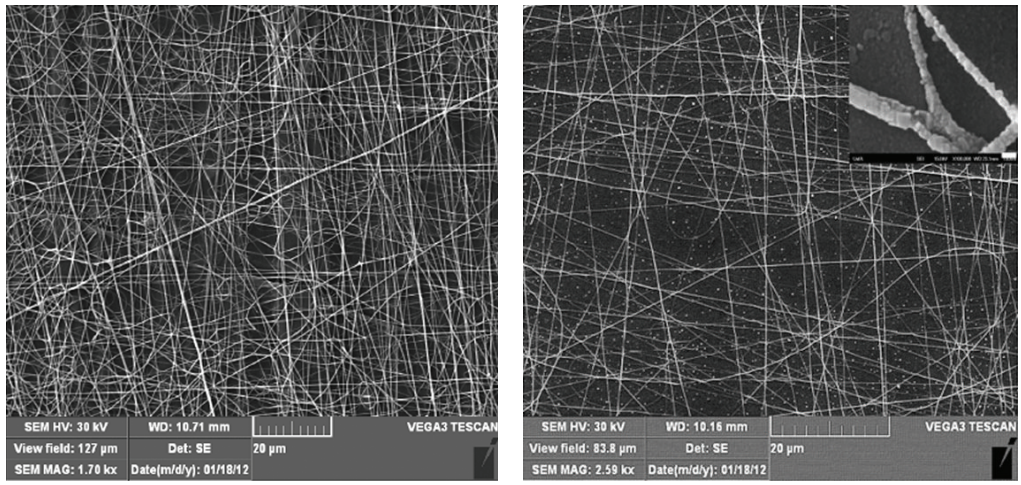

(a) (b)

Figure 1: SEM image of (a) as-spun nanofibers of BFO/Nylon6 prior to calcination. The image indicates the formation of continuous cylindrical nanofibers. (b) BFO nanofibers after calcination at 600°C. The integrity of the nanofibers is intact after the elimination of Nylon6; the inset shows FE-SEM image of the BFO nanofibers after calcination at 600°C with the scale bar indicating 100 nm. BFO nanofibers contain BFO crystallite with the mean size of 29 nm.

for SEM analysis were sputtered with gold. Field emission scanning electron microscopy (FE-SEM, JAMP-9500F, JEOL, USA) was utilized to determine the crystallite size on the nanofibers; the accelerating voltage of the microscope was set to 15 kV. The band gap of the BFO nanofibers was investigated by means of UV-Vis spectroscopy (Varian Carey 50, Agilent, USA).

2.5. Water Purification Studies. The application of the photocatalytic properties of BFO nanofibers in water purification was studied through the photo-degradation of 4CP. BFO nanofiber samples on 1.5 cm × 3 cm aluminum substrates weighing 0.5–0.7 mg were suspended in aqueous solutions with 4CP concentrations of 1, 2, 5 and 7.5 μg/mL in Milli-Q water. These samples were named 4CP-1, 4CP-2, 4CP-3 and 4CP-4, respectively. The samples were subsequently irradiated by UV light at a wavelength of 385 nm and an intensity of 15 W/cm^2 using a UV lamp (BlueWave LED Prime UVA, Dymax, USA). Two reference samples of 5 μg/mL were also prepared with no added BFO nanofibers; one was irradiated with UV light to determine the effectiveness of the nanofibers in the photo-degradation of 4CP (4CP-blank) and the other was left in the dark to see the role of UV irradiation on its own (4CP-dark). In order to guarantee the mass transfer of the contaminant to the surface of the nanofibers, all the water purification studies were conducted as the aqueous solutions were being magnetically stirred. At predetermined time intervals, 1 mL samples were taken from the aqueous solutions for further analysis using UV-Vis spectroscopy at 225 nm; the concentration of the contaminant was obtained by converting the absorbance values from the calibration curve of 4CP.

3. Results and Discussions

3.1. Characterization of the Nanofibers. Figure 1(a) shows the SEM image of the as-spun Nylon6/BFO fibers prior to calcination. The formation of continuous cylindrical nanofibers is evident, and the average diameter of the as-spun fibers was calculated to be 230 ± 30 nm. The continuousness of the BFO fibers was not compromised after calcination at 600°C as seen from SEM image in Figure 1(b); with Nylon6 no longer surrounding the BFO nanofibers, the average diameter was decreased to 130 ± 35 nm. The FE-SEM image in the inset of Figure 1(b) shows the BFO crystallites forming continuous nanofibers, and the average diameter of the crystallites is 29 ± 2 nm.

Although the high-temperature calcination guarantees the evaporation of the Nylon6 polymer and crystallization of BFO, to confirm the phase purity of calcinated BFO nanofibers, XRD analysis was carried out. The XRD pattern demonstrated the key characteristic peaks of R3C rhombohedral perovskite BFO matching the reported standard values (JCPDS: 01-071-2494). Peaks matched with platinum are resultant of the platinum-coated substrate, and small traces of the secondary phase $Bi_2Fe_4O_9$ can be distinguished. However, the dominant phase remains to be BFO (Figure 2).

To determine the band gap of the nanofibers, UV-Vis spectroscopy was utilized; absorption coefficient α and energy band gap E_g follow the correlation in (1), where β is the number indicative of the nature of the electron transition from the valance to the conduction band, h is Planck's constant, and k is a constant:

$$\alpha = \left(\frac{k}{h\nu}\right)\left(h\nu - E_g\right)^{\beta} \quad (1)$$

see [22].

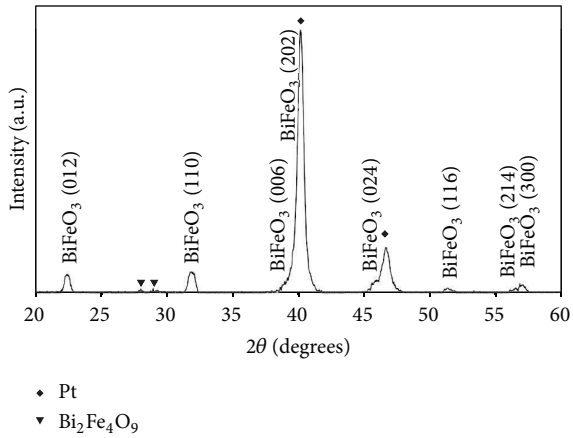

Figure 2: XRD pattern of the calcinated nanofibers showing the dominant presence of BFO. Platinum peaks are due to the Pt-coated substrate, and small traces of $Bi_2Fe_4O_9$ are found.

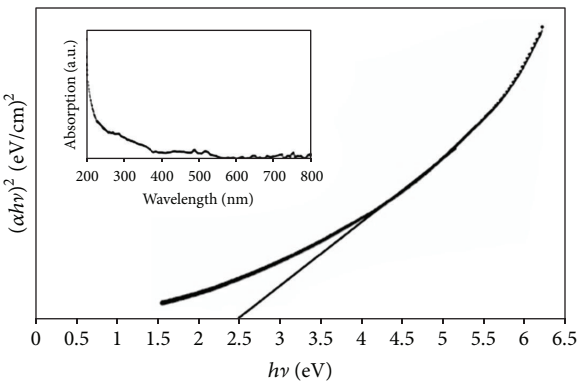

Figure 3: Band gap calculations for BFO nanofibers revealed the band gap energy of 2.5 eV. The inset shows the absorbance of the nanofibers for the irradiation by the light in a range of 200–800 nm.

For a material exhibiting a direct band gap, β is 1/2 and (1) can be written as (2) in which C is a constant:

$$(h\nu\alpha)^2 = C\left(h\nu - E_g\right) \tag{2}$$

see [22].

Ergo, the direct band gap of the BFO nanofibers, is obtained by the intercept of the linear portion of $(h\nu\alpha)^2$ versus $(h\nu)$. As depicted in Figure 3, the intercept suggests that the direct band gap of the BFO nanofibers is approximately 2.5 ± 0.05 eV, which is in agreement with reported values from studies by Ihlefeld et al. [16] and Hauser et al. [17], as mentioned previously, as well as Prashanthi et al. [23]. The inset in Figure 3 illustrates the absorption data acquired for the nanofibers by UV-Vis spectroscopy.

3.2. Water Purification. The value observed for the band gap of BFO suggests that the photocatalytic activity of the BFO nanofibers is expected to be observed under UV irradiation as well as UV-visible range irradiation; however, in this study UV irradiation at a wavelength of 385 nm was used in order to provide more photons with sufficient energy to ensure the photodegradation of the contaminant 4CP more efficiently, compared to visible irradiation. Figure 4(a) represents the relative change in the concentration of the contaminant 4CP in water for all 6 samples. The photocatalytic activity of the nanofibers is evident due to the fact that the reference sample 4CP-blank shows little signs of degradation over the testing period. This small change in the concentration is attributed to the direct photolysis caused by UV light since the reference sample 4CP-dark has demonstrated no change in concentration over the entire 360 min test duration. It has been established by Bertelli and Selli that 2CP, another member of the chlorophenol family, is almost photostable in water under irradiation in the wavelength range of 315–400 nm; in the absence of any photocatalysts, however, direct photolysis of this matter could happen under the irradiation at a much lower wavelength (254 nm) which is believed to be a direct consequence of C–Cl bond cleavage [24]. This is consistent with the data acquired from the UV light used in this study with an irradiation wavelength of 385 nm.

Table 1: Kinetics parameters for 4CP degradation based on the pseudo-first-order kinetics.

Samples	K (min^{-1})	R^2
4CP-1	−0.0317	0.9838
4CP-2	−0.014	0.9228
4CP-3	−0.0027	0.9416
4CP-4	−0.0018	0.8807

Figure 4(a) also implies that for samples 4CP-1 and 4CP-2 full degradation of the contaminant occurs in 90 min and 175 min, respectively; in the case of 4CP-3 and 4CP-4, however, the declining change in contaminant concentration only continues up to 60 min and 120 min of UV irradiation, correspondingly. The halt in the photocatalytic activity of the nanofibers was speculated to be due to the saturation of the nanofiber surface by the relatively high concentration of the contaminant. To investigate this hypothesis, samples with an initial concentration of 5 μg/mL that were irradiated for 240 min (named as 4CP-sat) were removed from the system, and the BFO nanofiber mats were rinsed with Milli-Q water. The mats were then returned to the solutions and UV irradiation was continued. As Figure 4(b) illustrates, the photocatalytic activity of the BFO was resumed after the nanofibers were rinsed and the degradation of 4CP-sat was completed in an additional 180 min. This confirms the hypothesis of surface saturation of the nanofibers.

In order to determine the governing kinetics of the degradation reactions of 4CP, the following pseudo-first-order model is proposed:

$$\ln\left(\frac{C_0}{C}\right) = kt, \tag{3}$$

where t represents irradiation time, k is the reaction rate constant, and C_0 and C are the initial concentration of the contaminant and the concentration of the 4CP at a given time, respectively; see [25]. According to the nearly linear behavior of $\ln(C/C_0)$ versus t for 4CP-1, 4CP-2, 4CP-3, and 4CP-4

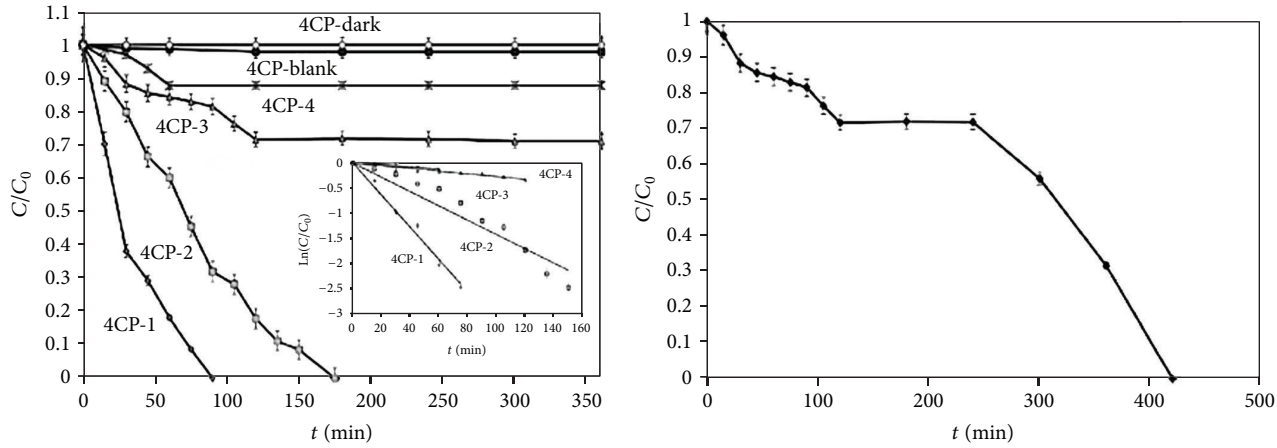

Figure 4: (a) The degradation of 4CP in contact with BFO nanofibers as a result of irradiation by the light with the wavelength of 385 nm. The gradual decrease in the different concentrations (1, 2, 5, and 7.5 μg/mL) of 4CP compared to the insignificant change in concentration for 4CP-blank and 4CP-dark is depicted. The inset illustrates the application of pseudo-first-order kinetics for the degradation of the 4CP, (b) the degradation of 4CP for 4CP-sat sample. The trend shows a stop in the degradation process at 120 min probably due to surface saturation, and it is resumed after the BFO nanofiber mat is rinsed.

in their degradation period given in the inset of Figure 4(a) and R^2 values reported in Table 1, the suggested model fits the photodegradation data of 4CP in the presence of BFO nanofibers with close approximation.

Table 1 also shows the reaction rate constant values calculated by applying the pseudo-first-order model as well as the R^2 values of the linear fit. It could be hypothesized that the decrease in the reaction rate constant with the increase in the contaminant concentration is due to the higher amount of saturated sites on the surface of the BFO nanofibers at higher 4CP concentration, therefore, reducing the number of active sites for the photocatalytic reaction to occur.

4. Conclusions

One-dimensional BFO nanofibers with an average fiber diameter of 130 ± 35 nm and average BFO crystallite size of 29 ± 2 nm were successfully fabricated through electrospinning and subsequent calcination at 600°C. SEM images confirmed the formation of the Nylon6/BFO nanofibers prior to calcination and the continuous BFO nanofibers after high-temperature calcination. Moreover, the band gap energy was calculated to be 2.5 eV. The photocatalytic activity of BFO nanofibers was evident from the photodegradation of the pollutant 4CP under UV irradiation. The proposed pseudo-first-order kinetics model deemed appropriate for the degradation of the contaminant. The results show promise for the application of BFO nanofibers in water purification due to a relatively low band gap energy that facilitates photoactivation. Furthermore, the nanofiber structure holds the advantage of the elimination of the extra filtration stage of photocatalyst itself after the degradation process is complete [26].

Conflict of Interests

The authors do not have any direct financial relation with the commercial identity mentioned in the paper that might lead to a conflict of interests.

Acknowledgment

This work was supported by Canada Excellence Research Chairs (CERC) Program. The authors would like to extend their gratitude towards the Nanofabrication Lab, Alberta Centre for Surface Engineering & Sciences (ACSES), and Oil Sands and Coal Interfacial Engineering Facility (OSCIEF) for characterization experiments.

References

[1] T. Ternes and U. von Gunten, "Editorial to special issue in Water Research. Emerging contaminants in water," *Water Research*, vol. 44, no. 2, p. 351, 2010.

[2] N. Savage and M. S. Diallo, "Nanomaterials and water purification: opportunities and challenges," *Journal of Nanoparticle Research*, vol. 7, no. 4-5, pp. 331–342, 2005.

[3] M. Iscan, "Hazard identification for contaminants," *Toxicology*, vol. 205, no. 3, pp. 195–199, 2004.

[4] H. F. Schröder, "Selective determination of non-biodegradable polar, organic pollutants in waste water related to functional groups using flow injection combined with tandem mass spectrometry," *Water Science and Technology*, vol. 34, no. 7-8, pp. 21–28, 1996.

[5] R. Hernandez, M. Zappi, J. Colucci, and R. Jones, "Comparing the performance of various advanced oxidation processes for treatment of acetone contaminated water," *Journal of Hazardous Materials*, vol. 92, no. 1, pp. 33–50, 2002.

[6] N. Keller, G. Rebmann, E. Barraud, O. Zahraa, and V. Keller, "Macroscopic carbon nanofibers for use as photocatalyst support," *Catalysis Today*, vol. 101, no. 3-4, pp. 323–329, 2005.

[7] J. M. Herrmann, "Heterogeneous photocatalysis: fundamentals and applications to the removal of various types of aqueous pollutants," *Catalysis Today*, vol. 53, no. 1, pp. 115–129, 1999.

[8] M. S. Lee, S. S. Park, G. D. Lee, C. S. Ju, and S. S. Hong, "Synthesis of TiO_2 particles by reverse microemulsion method using nonionic surfactants with different hydrophilic and hydrophobic group and their photocatalytic activity," *Catalysis Today*, vol. 101, no. 3-4, pp. 283–290, 2005.

[9] M. Hussain, R. Ceccarelli, D. L. Marchisio, D. Fino, N. Russo, and F. Geobaldo, "Synthesis, characterization, and photocatalytic application of novel TiO_2 nanoparticles," *Chemical Engineering Journal*, vol. 157, no. 1, pp. 45–51, 2010.

[10] S. Chuangchote, J. Jitputti, T. Sagawa, and S. Yoshikawa, "Photocatalytic activity for hydrogen evolution of electrospun TiO_2 nanofibers," *ACS Applied Materials & Interfaces*, vol. 1, no. 5, pp. 1140–1143, 2009.

[11] Z. Liu, X. Zhang, S. Nishimoto, T. Murakami, and A. Fujishima, "Efficient photocatalytic degradation of gaseous acetaldehyde by highly ordered TiO_2 nanotube arrays," *Environmental Science and Technology*, vol. 42, no. 22, pp. 8547–8551, 2008.

[12] K. Sunada, Y. Kikuchi, K. Hashimoto, and A. Fujishima, "Bactericidal and detoxification effects of TiO_2 thin film photocatalysts," *Environmental Science and Technology*, vol. 32, no. 5, pp. 726–728, 1998.

[13] X. H. Xia, Y. Liang, Z. Wang, J. Fan, Y. S. Luo, and Z. J. Jia, "Synthesis and photocatalytic properties of TiO_2 nanostructure," *Materials Research Bulletin*, vol. 43, no. 8-9, pp. 2187–2195, 2008.

[14] S. K. Choi, S. Kim, S. K. Lim, and H. Park, "Photocatalytic comparison of TiO_2 nanoparticles and electrospun TiO_2 nanofibers: effects of mesoporosity and interparticle charge transfer," *Journal of Physical Chemistry C*, vol. 114, no. 39, pp. 16475–16480, 2010.

[15] G. Laera, B. Jin, H. Zhu, and A. Lopez, "Photocatalytic activity of TiO_2 nanofibers in simulated and real municipal effluents," *Catalysis Today*, vol. 161, no. 1, pp. 147–152, 2011.

[16] J. F. Ihlefeld, N. J. Podraza, Z. K. Liu et al., "Optical band gap of $BiFeO_3$ grown by molecular-beam epitaxy," *Applied Physics Letters*, vol. 92, no. 14, Article ID 142908, 2008.

[17] A. J. Hauser, J. Zhang, L. Mier et al., "Characterization of electronic structure and defect states of thin epitaxial $BiFeO_3$ films by UV-visible absorption and cathodoluminescence spectroscopies," *Applied Physics Letters*, vol. 92, no. 22, Article ID 222901, 2008.

[18] S. Li, Y. H. Lin, B. P. Zhang, C. W. Nan, and Y. Wang, "Photocatalytic and magnetic behaviors observed in nanostructured $BiFeO_3$ particles," *Journal of Applied Physics*, vol. 105, no. 5, Article ID 056105, 2009.

[19] X. Xu, Y. H. Lin, P. Li, L. Shu, and C. W. Nan, "Synthesis and photocatalytic behaviors of high surface area $BiFeO_3$ thin films," *Journal of the American Ceramic Society*, vol. 94, no. 8, pp. 2296–2299, 2011.

[20] F. Gao, X. Chen, K. Yin et al., "Visible-light photocatalytic properties of weak magnetic $BiFeO_3$ nanoparticles," *Advanced Materials*, vol. 19, no. 19, pp. 2889–2892, 2007.

[21] E. Leyva, E. Moctezuma, M. G. Ruíz, and L. Torres-Martínez, "Photodegradation of phenol and 4-chlorophenol by BaO-Li_2O-TiO_2 catalysts," *Catalysis Today*, vol. 40, no. 4, pp. 367–376, 1998.

[22] N. Shakti and P. S. Gupta, "Structural and optical properties of sol-gel prepared ZnO thin film," *Applied Physics Research*, vol. 2, no. 1, pp. 19–28, 2010.

[23] K. Prashanthi, G. Thakur, and T. Thundat, "Surface enhanced strong visible photoluminescence from one-dimensional multiferroic $BiFeO_3$ nanostructures," *Surface Science*, vol. 606, pp. L83–L86, 2012.

[24] M. Bertelli and E. Selli, "Reaction paths and efficiency of photocatalysis on TiO_2 and of H_2O_2 photolysis in the degradation of 2-chlorophenol," *Journal of Hazardous Materials*, vol. 138, no. 1, pp. 46–52, 2006.

[25] K. V. Baiju, S. Shukla, K. S. Sandhya, J. James, and K. G. K. Warrier, "Photocatalytic activity of sol-gel-derived nanocrystalline titania," *Journal of Physical Chemistry C*, vol. 111, no. 21, pp. 7612–7622, 2007.

[26] I. Poulios and I. Tsachpinis, "Photodegradation of the textile dye Reactive Black 5 in the presence of semiconducting oxides," *Journal of Chemical Technology and Biotechnology*, vol. 74, pp. 349–357, 1999.